Wake Characteristics of Large-scale Wind Turbines

Yaxing Wang, Vladimir Leble, Mark White and George N. Barakos

School of Engineering, University of Liverpool, L69 3GH, U.K.
Email: yxwang@liverpool.ac.uk

Abstract

The next generation of large-scale wind turbines will exceed 10 MW of rated power and will reach rotor diameters of about 200 m. Their rotor aerodynamics are also extreme with Reynolds numbers that reach 40 million. The wakes generated by these wind turbines cover a very large area downstream of their installation positions which increases the possibility that the wake vortices generated by these large wind turbines may affect passing-by flying vehicles. In this paper a CFD study of a large wind turbine was carried out to predict the power curves and aerodynamic loads on the rotor blades. Flow control devices of active leading and trailing edge flaps were also considered in the CFD study and the effects of flaps were investigated. The near wake flow was captured in the CFD study and the flaps add more complexity to the wake flow. To study the potential wind turbine wake encounters by aircraft, engineering wake models were developed to predict the wind turbine far wakes. The wake induced velocity fields were integrated into an aircraft flight dynamics model to simulate wind turbine wake encounter scenarios, designed for a light aircraft approaching an airport, where a wind turbine is installed. The severity of the wind turbine wake encounter was analysed using off-line flight simulations. The off-line simulation results indicated that the wake encounter severity was highly dependent on the ways that the wake vortex circulation and the core size were calculated, which suggested that field measurements of large wind turbines wake flow are needed to verify the modelling and CFD results.

1 INTRODUCTION

The wake vortices generated by a wind turbine or a wind farm have similar, but not identical, characteristics as aircraft wake vortices. The next generation of large-scale wind turbines will exceed 10 MW of rated power and will reach rotor diameters of about 200 m [1]. The rotor aerodynamics are also extreme with Reynolds numbers reaching 40 million. The wakes generated by these wind turbines cover a very large area downstream of their installation positions which increases the possibility that the wake vortices generated by these large wind turbines may affect passing-by flying vehicles. In the past, the University of Liverpool (UoL) has studied the wake encounters between relatively small wind turbine wakes and light GA aircraft using engineering modelling, CFD, LIDAR field measurements and piloted flight simulations [13].

The advent of the large-scale wind turbines presents new challenges not only for the CFD study of wind turbine performance and prediction of aerodynamic loads, but also for the wind turbine wake evaluations.

To obtain realistic wake data may be difficult unless high resolution CFD is used [5]. This is not only due to the large scale wake but also due to the complexity of the flow caused by flaps on the blades. Flaps are to be used on these large-scale wind turbines to control the flow and alleviate aerodynamic loads. The flaps will produce their own tip vortices and the wake now is difficult to predict with engineering wake models.

UoL is participating in the European project AVATAR concerning the development of next generation very large wind turbines with a power output of 10 MW. Advanced aerodynamic CFD studies were conducted to predict the power curves and detailed loads of such wind turbines.

In the UK wind turbines are being proposed and built close to aerodromes, indicating an urgent need to assess the potential impact of wake turbulence on aircraft and in particular, to light aircraft and helicopters [3]. So the understanding and prediction of wind turbine wake characteristics are vital to prevent flight accidents during wind turbine wake encounters.

Wind turbine wakes can be divided into near and far wake regions [10, 12]. The near wake is the area just behind the rotor up to approximately one rotor diameter downstream, where the effect of rotor properties, including the blade aerodynamics and geometry determine the flow field. Near wake research is focused on the wind turbine performance and the physics of power extraction. The far wake is the region beyond the near wake, where the details of the rotor are less important. The main interest in this area is the wake interference with other wind turbines (wind farm) or passing-by aircraft (wind turbine wake encounter). Here, the flow convection and turbulent diffusion are the two main mechanisms that determine the far flow field.

There are similarities between helicopter rotor wakes and wind turbine wakes and the vortex methods that are used for the analysis of helicopter wake problems can be adopted to represent the strengths and the spatial locations of the vortical wake elements that are trailed by each blade and convected

into downstream. Prescribed vortex wake models [6] have also been developed for wind turbine applications. Like the helicopter rotor wake cases, the models are usually based on the assumption of incompressible, potential flow, and experimental observations. The free wake model [7, 8] determines the wake shape based on the local velocity field, and the wake structure is represented by a large number of free vortex filaments. These filaments can propagate freely in the induced velocity field. Its solution can only be obtained by iterations.

CFD simulation of wind turbine wakes is an active area of research, and with increasing computer power, grid-based CFD simulation of wind turbine from Navier–Stokes (NS) equations are practical. However, the far wake simulation needs fine grid resolution. Actuator disk [10, 12] and actuator line [11] methods were used to simulate the rotor and the rest of flow was simulated by solving the NS equations, which enabled the CFD domain to cover the region extending from rotor plane to several diameters downstream to study both the near and far wake development. Recently, full CFD methods [4, 5] were used to study the wake development and breakdown. These methods are very computationally expensive and require fine grids to cover the far wake region. In most CFD wake studies, the flow conditions were treated as ideal. The effects of wind shear, terrain and ambient turbulence were normally ignored. This results in predictions that show much stronger and coherent vortices.

For large wind turbines, the full CFD simulation of wind turbine far wake requires very fine grid and large domain covering a long distance (at least 4D-5D) downstream to capture the detailed physics of the wake evolutions. This restriction makes the full CFD study of a wind turbine wake deemed to be impractical, especially for the generation of wake database for the flight simulations. To this end, engineering models with reasonable accuracy and low computational cost were sought. The Kocurek wake model and freewake model were developed and validated with available measurements.

The velocity data generated by the models were applied in the off-line flight simulations to study the wake hazard severity when a light aircraft configured based on a Grob Tutor aircraft, encounters the wind turbine wake. The Kocurek model and the free wake model were applied for large wind turbines for the generation of wake induced flow.

In this paper, CFD results on the next generation large wind turbines are introduced. The power output and the aerodynamic loads on rotor blades were evaluated, and the effects of trailing and leading edge oscillating flaps on blade loads and flow were investigated. The near wake characteristics of the wind turbine are presented and compared with and without the actions of flaps.

Different engineering wind turbine wake models that were used in the previous wake studies were applied to the large wind turbine. Off-line flight simulations were carried out to analyse the hazard severity when a GA aircraft encountered these large wind turbine wakes.

2 CFD SIMULATION OF THE AVATAR WIND TURBINE

AVATAR is the next generation wind turbine developed for power output of 10 MW. The rotor diameter reaches to 205.8m. To predict the performance and potential flow control devices in the form of active flaps, CFD analyses of the AVATAR wind turbine have been conducted. The Helicopter Multi-Block (HMB2) solver developed at Liverpool University was used to estimate the aerodynamic forces and blade deformation. The HMB2 solver has so far been validated for several wind turbine cases, including the NREL and Mexico project [4] experiments.

2.1 Numerical methods

The HMB2 code is a 3D multi-block structured solver and solves the Navier-Stokes equations in the 3D Cartesian frame of reference. HMB2 solves the Navier-Stokes equations in integral form using the arbitrary Lagrangian-Eulerian formulation for time-dependent domains with moving boundaries. The solver uses a cell-centred finite volume approach combined with an implicit dual-time method. The Osher upwind scheme is used to resolve the convective fluxes. Central differencing (CD) spatial discretisation method is used to solve the viscous terms. The non-linear system of equations that is generated as a result of the linearisation is then solved by integration in pseudo-time using a first-order backward difference method. A Generalised Conjugate Gradient (GCG) method is then used in conjunction with a Block Incomplete Lower-Upper (BILU) factorisation as a pre-conditioner. The HMB2 solver has a library of turbulence closures including several one-equation and two-equation turbulence models, and turbulence simulation is also possible using either the Large-Eddy or the Detached-Eddy simulation approach. The solver was designed with parallel execution in mind and the MPI library along with a load-balancing algorithm are used to this end. The flow solver can be used in serial or parallel fashion for large-scale problems. Depending on the purposes of the simulations, steady and unsteady wind turbine CFD simulations can be performed in HMB2 using single or full rotor meshes generated using the ICEM-Hexa tool. Rigid or elastic blades can be simulated using static or dynamic computations. To account for low-speed flows, the Low-Mach Roe scheme (LM-Roe) [4] was developed for wind turbine cases.

2.2 CFD results

2.2.1 Power and loads predictions

First, steady and unsteady computations were preformed assuming rigid blades. The thrust and mechanical power as function of wind speed are presented in Figure 1. The k-ω SST turbulence model was employed for the computations. The computation domain included a single blade taking advantage of the flow periodic in the space. The grid size was 9.7M cells with an initial wall distance of 10^{-6} of the blade maximum chord to resolve the thin boundary layers. The results were compared with that of different CFD solvers used by various AVATAR partners and relatively good agreement was achieved. As can be seen the thrust values are far beyond the conventional wind turbines.

2.2.2 Flow and loads controls by leading and trailing edge flaps

The AVATAR blades were equipped with leading and trailing edge flaps. The leading edge (LE) flap was located at 60%R station, and the trailing edge (TE) flap was located at 75%R. The length of each flap was 10%R, but the width of the TE flap was 10% of the local chord, whereas the width of the LE flap was 20% of the local chord, as shown in Figure 2 . The flaps are deflected form -10° to 10° with the shape and notation presented in Figure 2. Two frequencies of flap motion were studied at 0.16Hz (once per revolution) and 0.96Hz (six times per revolution). The inflow wind speed was 11.4m/s.

The span-wise load distributions for active trailing and leading edge flap are shown in Figures 3 and 4. As can be seen, the flap deflection has a localised effect on the loads distribution i.e. it does not affect the whole span of the blade. The TE flap has a higher influence on thrust force, driving force and pitching moment, as compared to the LE flap. Clearly, the actuated LE and TE flaps can be seen as a mechanism to locally change the loads acting on the blade.

2.2.3 Near wake flow fields generated by blades and leading and trailing edge flaps

The CFD study in the AVATAR project was focused on the prediction of performance, so only the near wake was taken into consideration. The near wake flow is shown in Figures 5 for the clean blades. Figure 6 shows the near wake flow when a trailing edge flap is activated. The wake vortices are indicated by the iso-surfaces of the λ_2 criterion. The wake vortices trailed from the blade tip and two side edges of the flap were clearly indicated. Compared with the clean blade cases [4], the presence of flap added more complexity of wake flow and the wake vortices of flap showed same level of strength as that of the blade tip vortex.

3 WIND TURBINE WAKE MODELLING

Modelling wind turbine wakes requires accurate prediction and simulation of wake vortex geometry, wake breakdown, mean velocity deficits and wake induced velocity flow-fields. There are several wake models available in the literature [10, 12] with different levels of complexity and fidelity. Two wake modelling methods are used in this study. These are the Kocurek wind turbine wake vortex model and the free wake model.

3.1 Kocurek wind turbine wake vortex model and validation

The wind turbine wake was firstly modelled using the modified Kocurek wind turbine wake vortex model [6] to capture the location and strength of the tip vortices. The Kocurek wind turbine wake vortex model developed at UoL was validated with wind tunnel measurements of the MEXICO wind turbine [13]. This model was also applied to a WTN250 wind turbine (diameter 30 m), where field LIDAR measurements were available.

With the availability of the CFD results of the AVATAR wind turbine, the Kocurek wake model was able to be applied

to the AVATAR rotor using the thrusts calculated by CFD at different wind speeds.

Figure 7 shows the geometries of the tip vortices generated by each blade and the contours of the axial induced velocities. The induced flow shows similar pattern as those of the smaller wind turbine [13].

3.2 Free wake model for wind turbine

In the free wake model [7, 8], the initial geometry of the wake is first assumed. The wake itself is represented by a large number of free vortex filaments. These filaments can propagate freely in the induced velocity field. A free wake model has been developed in this study to account for ground effect. The tip and root vortices were simulated. The rotor thrust was estimated from the blade element momentum (BEM) to calculate the circulation of the blade. The self-induced flow and the local wake curvature, are considered in the formulation. The velocity field is estimated using the Biot-Savart law. Ground effect is simulated by using a mirror wake with respect to the ground plane [8]. Figures 8 show iso-surfaces of vorticity indicating the positions of the vortex cores, as predicted by the free wake model. At a low wind speed of 7 m/s, the wake shows instabilities after a distance of 1.5D downstream.

4 OFF-LINE FLIGHT SIMULATION OF WIND TURBINE WAKE ENCOUNTER

4.1 Wake encounter scenarios

The wind turbine wake encounter scenario was designed for a light aircraft approaching an airport, where a large wind turbine was installed. The wind turbine wake might generate upsets on the passing-by aircraft. The wind turbine rotor hub was positioned at a height of 1D above the ground and at several offsets from the centerline of the runway at orientation angles of 90° and 45°. The wake encounter scenario is illustrated in Figure 9 where the light aircraft is penetrating the wind turbine wake during approaching an airport during 45° oblique encounter.

In the off-line analysis, the GA aircraft was set to fly at different positions relative to the wind turbine location. The aircraft was first put outside the wake flow field and trimmed initially at a flight condition of 70 kts, as used in the piloted flight simulations. Then, all body states were frozen during the off-line simulations. The total forces and moments on the aircraft can be obtained by summing all the forces and moments on the individual components. The variations of forces or moments when the aircraft was outside and in the wake flow can be used as an indication of the wake disturbance and the wake encounter severity of wind turbine wakes on an aircraft. Compared with the piloted flight simulation, the dynamic responses and the pilot controls and re-trimming were excluded in the off-line tests, which represent the quasi-steady acceleration as if the aircraft were instantaneously placed in the wake.

The large wind turbine rotor used in the off-line simulation has a diameter of 90 m, which represents the size of the widely installed large wind turbines of 2-3 MW power output. The circulations at different wind speeds were calculated by

using the following Beddoes formula [2].

$$\Gamma/(cR\Omega) \;=\; 2.4 c_T/\sigma \qquad (1)$$

where $c_T = Thrust/(\rho\pi R^4\Omega^2)$, σ is the solidity of rotor blades, Ω is the rotation speed of the rotor and c is the chord of blades.

It can also be calculated by using scaling laws from a small wind tunnel wind turbine wake measurement [9].

The initial wake vortex core is set to be 5 percent of the averaged chord [2, 7]. In the off-line analysis the enlarged core size (20 percent chord) was also used to consider a worst-case-scenario.

In this paper, "model 1" and "model 2" are used to indicate that the Beddoes formula and the scaling laws circulation formula [9].

The decay of local wake vortex circulation Γ_i after time t can be calculated by

$$\Gamma_i/\Gamma_0 \;=\; exp(-Ct\Gamma_0/(2\pi b_0^2 T_c)) \qquad (2)$$

where Γ_0 is the initial circulation, b_0 is the vortex span, and C is a constant of 0.45. T_c is determined by

$$\epsilon^*(T_c)^{4/3} \;=\; 0.7475 \qquad (3)$$

$$\epsilon^* = 2\pi b_0/(\Gamma_0(\epsilon b_0)^{1/3}) \qquad (4)$$

where ϵ is the turbulent intensity. For a high turbulence case at the turbulent intensity of 10%, ϵ is 0.01.

The final circulation decay is

$$\Gamma_i/\Gamma_0 \;=\; exp(-Ct(\epsilon\Gamma_0)^{1/4}/(0.956(\pi)^{1/4}b_0)) \qquad (5)$$

4.1.1 Wake induced crosswinds of a large wind turbine

There is a limit on the magnitude of the allowed crosswind dependent on the airport and the aircraft. The wind turbine wake induced flow can be seen as crosswind to the encountering aircraft. The wake induced velocity fields were obtained on a large wind turbine using the Kocurek wake model. The dominant velocity component is the axial velocity U. The V and W velocities are one order of magnitude smaller than the U velocity. In the crossing or oblique encounters, the axial velocity constitutes the crosswind, which is one of the criteria used for evaluation of the encountering hazard. For an airport (codes A-I or B-I) that is expected to accommodate single engine aircraft, the maximum crosswind is 12.10 mph (17.75 ft/s) [9].

Two wind speeds of 32.8 ft/s and 65.6 ft/s were used in the off-line simulations. The wake induced crosswind speeds of this large wind turbine in the wake region are shown in Figure 10. The wake induced crosswind speeds calculated in model 1 are less than the criteria in the whole wake region; while in model 2, the induced crosswind speeds exceeded the crosswind criterion of the A-IV through D-VI airports in the region within 65D for the lower wind speed of 32.8 ft/s and in all region up to 100D for the higher wind speed of 65.6 ft/s.

4.1.2 Variations of forces and moments of the GA during wake encounters

For the GA aircraft based on the Grob Tutor configuration, the wing area $S_{wing} = 131.4 ft^2$ and the wind span $sp = 32.8 ft$. A flight speed $wf = 70kt$ ($118ft/s$) was used in the off-line simulations. The forces and moments were normalised by $0.5\rho wf^2 S_{wing}$ and $0.5\rho wf^2 S_{wing} sp$,respectively, to obtain the force and moment coefficients. The off-line simulation results of crossing encounters are shown in Figures 11 and 12, where variations of the forces and moments coefficients on the GA as it encountered the wind turbine wake along the runway central line at an offset of 3D were plotted. The figures show similar trends as the small wind turbine with a dominant yaw moment disturbance. However, the magnitudes of the coefficients of the forces and moments were much larger than that of a small wind turbine. The circulations calculated in model 2 were larger than these in model 1, and resulted in much large variations.

4.1.3 Analysis of the roll upsets during wake encounters

In the off-line flight simulation, the aircraft might have missed the positions where the induced velocities are large when it flew through the wake. So the off-line results of the rolling moment coefficient might not account for very localised peak velocities. In this section, an analytical method was adopted to calculate the rolling moment coefficients on the points of a fine grid in the wake field. The wake induced velocity components were extracted in the regions close to the rotor tip, where the induced velocities reach the maximum and minimum values with rapid changes. According to the report of [9], this is the area that the wake caused the largest roll upsets on the encountering aircraft. If the wake vortex core was assumed to be comparable with the aircraft wing span, and when the aircraft was positioned in the vortex center and was orientated with the vortex axis, the vortex produced upwash on one side of the wing and downwash on the other side, which resulted maximum induced velocities in the vertical direction and hence generated the largest roll moment on the aircraft. The same methodology of calculating the roll moment was also adopted here. The wake induced velocity components were obtained using a fine grid with resolution of 1 ft in the regions close to the vortex tip-path. The aircraft was configured to be flying in an orientation that the three velocity components could be treated as the vertical velocities on the wing. An integration of the induced velocities at the computing points was then carried out to obtain the roll moment coefficients at each position.

The contours of the wake induced rolling moment coefficients caused by the velocity components V_y and V_x are shown in Figure 13. A higher wind speed of 65.6 ft/s and the circulation formula of model 2, and an enlarged core size of 20 percent chord were used in the calculations of the wake induced rolling moment coefficients. This was considered to be the worst case scenario. The GA aircraft geometry is also plotted in the figure for comparison.

The peaks and valleys of the rolling moment coefficients were well captured by using the fine grid. The maximum rolling moment coefficients were approximately 0.06 and 0.1 induced by the velocity components V_y and V_x, respectively.

The criteria of the rolling moment coefficient is 0.28, which was calculated by considering the maximum rolling moment that the aileron on a normal aircraft can generate at the maximum deflection angle [9].

5 CONCLUSIONS AND FUTURE WORK

A CFD study of the next generation large (AVATAR) wind turbine of 10 MW was carried out to predict the power output and aerodynamic loads on the rotor blades. The effects of flow control devices in the form of trailing and leading edge flaps were investigated. The near wake characteristics of the AVATAR wind turbine were captured in the CFD predictions. However, based on the previous CFD study of the wind turbine wake breakdown, the far wake CFD study requires a very fine grid and a large computational domain covering a long distance (at least 4D-5D) downstream to capture the detailed physics of the wake evolutions. This restriction makes the full CFD study of wind turbine wake impractical, especially, for the generation of wake database for the flight simulations.

Different engineering wake models were sought to generate wake data with reasonable accuracy and low computation cost. A Kocurek wake model and a freewake model were developed and validated with available measurements. These models generated wake induced velocity fields with essential features. The velocity data generated by the models were applied to the off-line flight simulations to study the wake hazard severity when a light aircraft approximating a Grob Tutor aircraft, encounters the wind turbine wake.

The wake induced crosswinds were compared with the criteria of FAA [9] for different types of airports. The wake induced rolling moments on the encountering aircraft were analysed and compared with the rolling criterion which is based on the maximum roll moment produced by the aileron. The ways of calculation of wake vortex circulation and core size was found to play a vital role in the evaluation of wake encounter severity. The Beddoes circulation formula, which was developed for helicopter rotors and is supported by experimental evidence, produced less crosswind and rolling moments than those predicted by the scaling laws from a small wind tunnel experimental data. This suggested that field LIDAR measurements of large wind turbine wakes are needed to verify the wind turbine wake modelling, wake strength, decay and full CFD simulation results.

Piloted fight simulations are planned to put pilots in the loop to study the wake encounter severity on the encountering light aircraft and helicopters in the same fashion as that of the previous study of a small wind turbine wake encounters. Wind turbine wakes with higher spatial resolutions will be generated for both piloted and off-line flight simulations. Unsteady wakes with different turbulence intensities are planned to be implemented in future fight simulations.

COPYRIGHT STATEMENT

REFERENCES

[1] AVATAR Project. AVATAR next generation of large scale wind turbines, 2014.

[2] T.S. Beddoes. A Wake Model for High Resolution Airloads. *U.S. Army/AHS Conference on Rotorcraft Basic Research*, February 1985.

[3] CAA. CAA Policy and Guidelines on Wind Turbines. Technical report, Civil Aviation Authority, January 2012.

[4] M. Carrion, R. Steijl, M. Woodgate, and G. Barakos. CFD Analysis of the Wake of the MEXICO Wind Turbine. *Wind Energy*, 00:1–17, 2012.

[5] M. Carrion, M. Woodgate, R. Steijl, G. Barakos, S. Gomez-Iradi, and X. Munduate. Understanding Wind Turbine Wake Breakdown Using CFD. *Journal of AIAA*, Accepted, 2014.

[6] D. Kocurek. Lifting Surface Performance Analysis for Horizontal Axis Wind Turbines. Technical Report SERI/STR-217-3163, Solar energy research institute, US department of energy, 1987.

[7] G. Leishman. *Principles of Helicopter Aerodynamics*. Cambridge aerospace series book, Cambridge, UK, second edition, 2007.

[8] J.G. Leishman, M.J. Bhagwat, and A. Bagai. Free-Vortex Filament Methods for the Analysis of Helicopter Rotor Wakes. *Journal of Aircraft*, 39(5):759–775, 2002.

[9] T.E. Mulinazzi and Z.C. Zheng. Wind Farm Turbulence Impacts on General Aviation Airports in Kansas. Technical Report K-TRAN KU-13-6, Kansas State University, January 2014.

[10] B. Sanderse. Aerodynamics of Wind Turbine Wakes. Technical Report ECN-E-09-016, Energy research centre of the Netherlands, 2000.

[11] N. Troldborg, J.N. Sorensen, and R. Mikkelsen. Numerical Simulations of Wake Characteristics of a Wind Turbine in Uniform Inflow. *Wind Energy*, 13:86–99, 2010.

[12] L. Vermeer, J. Sorensen, and A. Crespo. Wind Turbine Wake Aerodynamics. *Progress in Aerospace Sciences*, 39:467–510, 2003.

[13] Y. Wang, M. White, G. Baracos, S. Wheeler, P. Tormey, and P. Pantazopoulou. Wind turbine wake encounter by light aircraft. In *40th European Rotorcraft Forum*, Southampton, UK, September 2014.
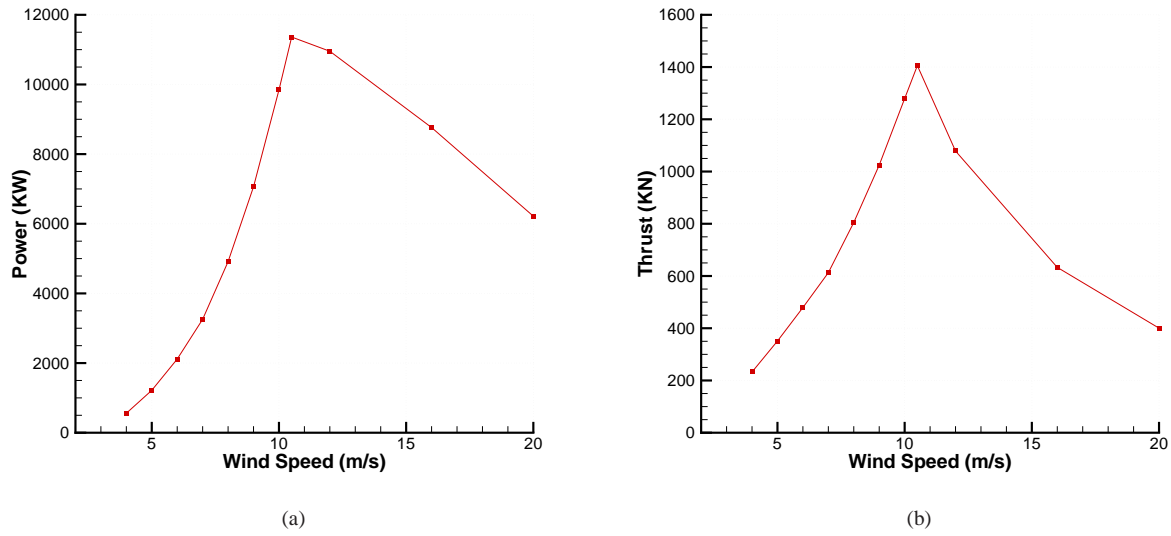
Figure 1: Power and thrust of the AVATAR wind turbine rotor, CFD simulation, rotor diameter 205.8 m with varying pitch and rotation speed.
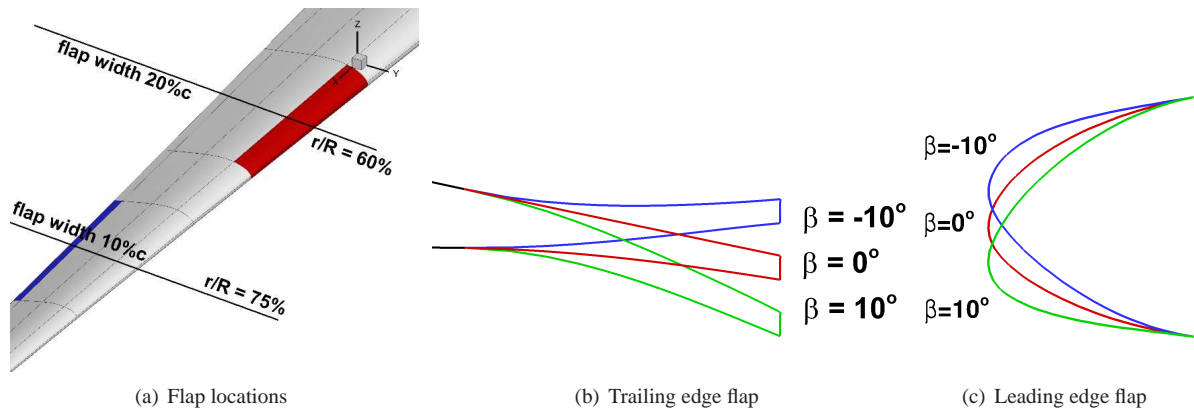

(a) Flap locations   (b) Trailing edge flap   (c) Leading edge flap

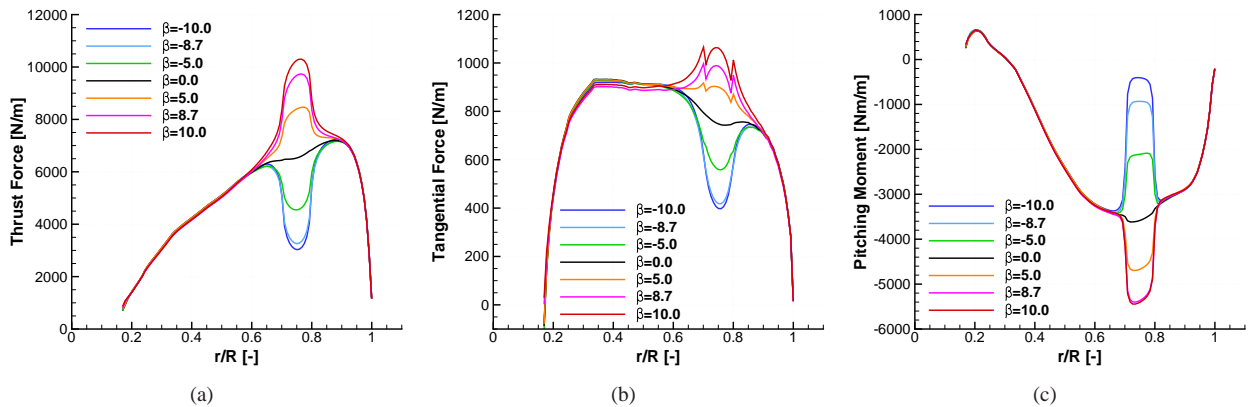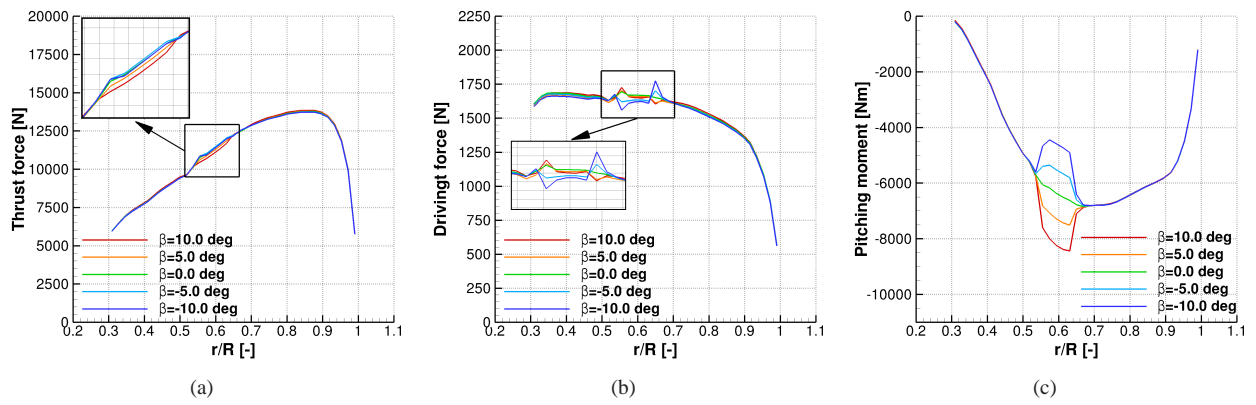Figure 2: Flap locations on the AVATAR wind turbine blade and flap deflections.

(a)   (b)   (c)

Figure 3: Spanwise distributions of forces and pitch moment of the AVATAR wind turbine blade with a trailing edge flap, wind speed 11.4 m/s, flap deflection range -10 deg to 10 deg at a frequency of 0.96Hz (6 Per rev).

6

Figure 4: Spanwise distributions of forces and pitch moment on the AVATAR wind turbine blade with a leading edge flap, wind speed 11.4 m/s, flap deflection range -10 deg to 10 deg at a frequency of 0.96Hz (6 6 Per rev).
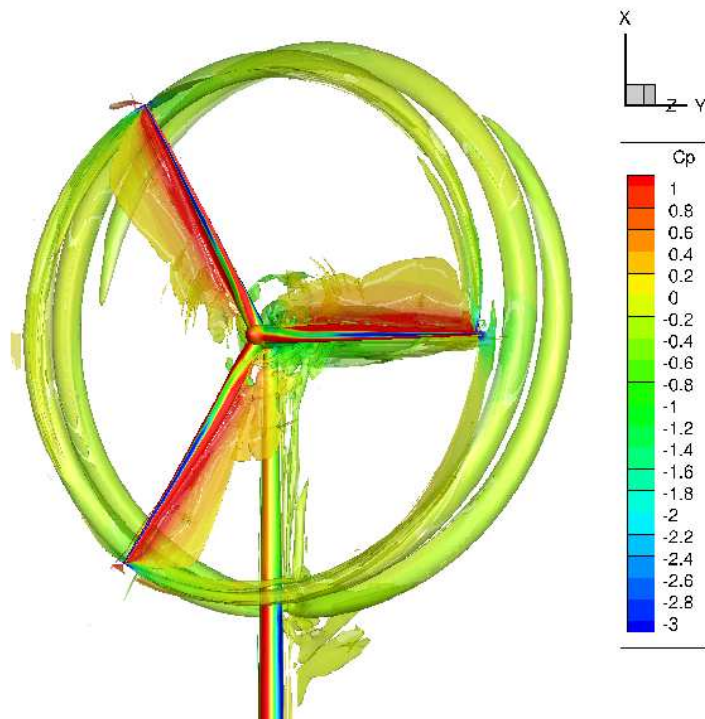
Figure 5: Iso-surfaces of Q=0.1 generated by clean blades and coloured using Cp.
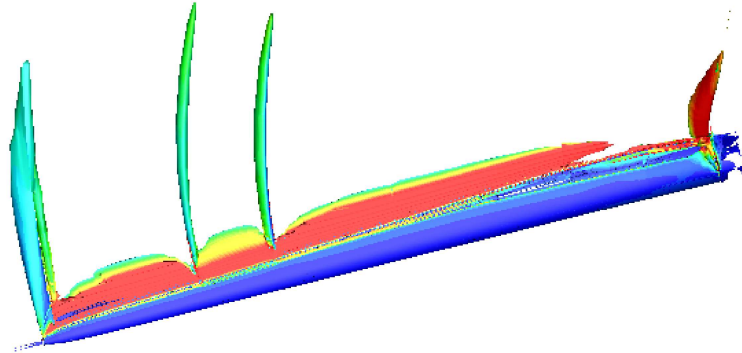
Figure 6: Contours of iso-surfaces of λ_2 of an AVATAR blade with an active trailing edge flap.
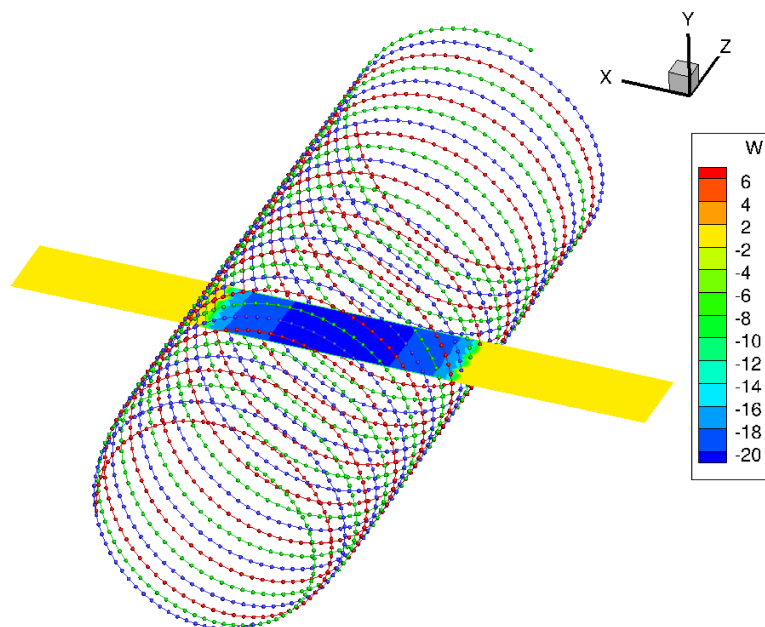
Figure 7: AVATAR wake geometries generated by Kocurek model at wind speed of 10.5 m/s.
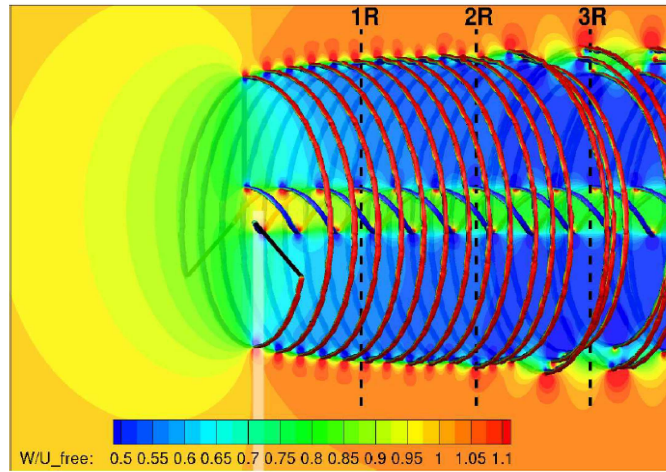
(a) Wind speed 7 m/s
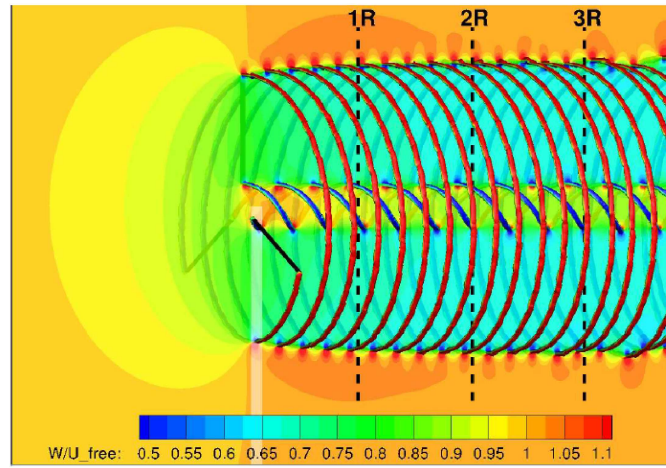
(b) Wind speed 10.5 m/s
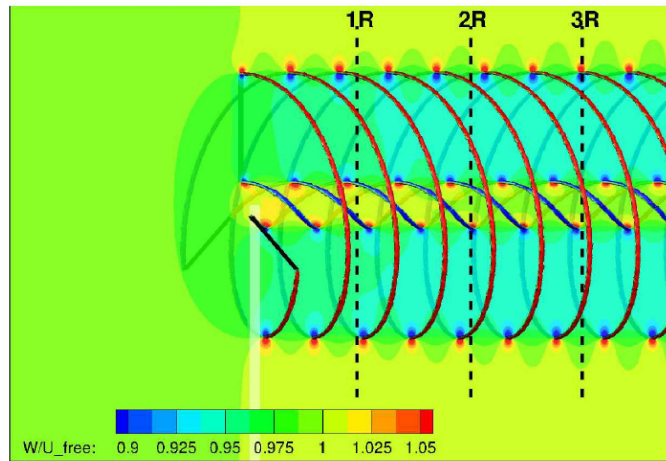
(c) Wind speed 20 m/s

Figure 8: Contours of iso-surfaces of vorticity and induced axial velocities predicted by free wake model at wind speeds of 7 m/s, 10.5 m/s and 20 m/s.
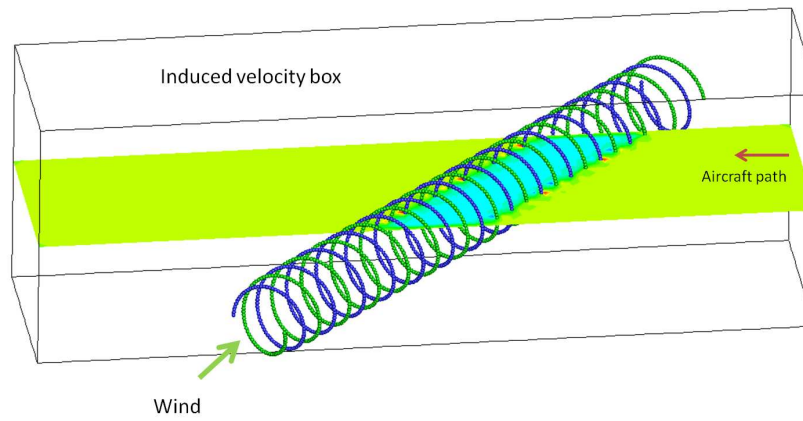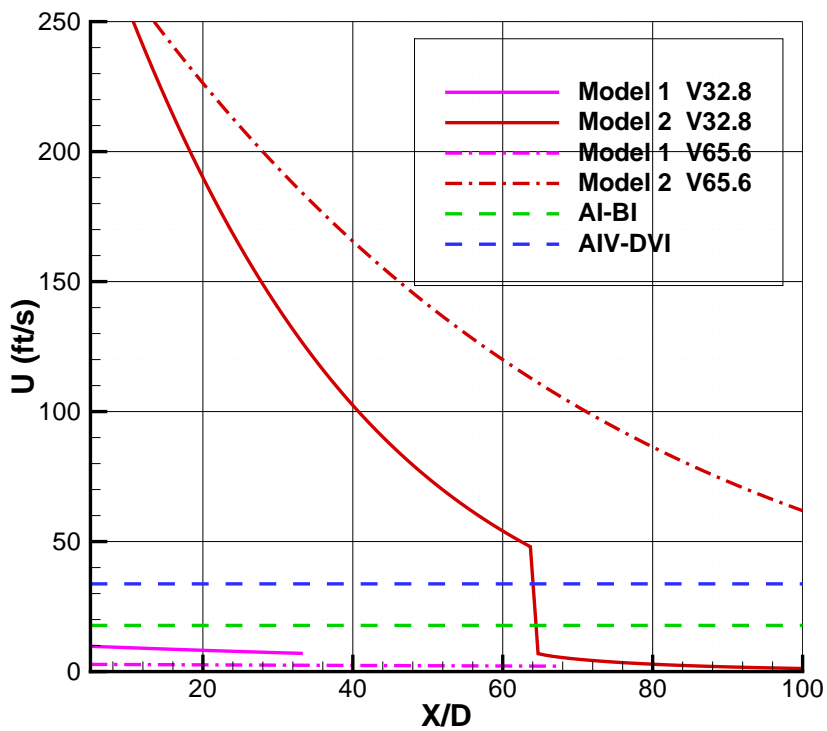
Figure 9: Oblique wind turbine (45°) wake encounter scenario.

Figure 10: Wake induced crosswind speeds against distances, 90 m diameter large wind turbine, wind speed 32.8 ft/s and 65.6 ft/s. AI-BI: airport codes expected to accommodate single engine aircraft; AIV-DIV: airport codes for larger air carrier airports.
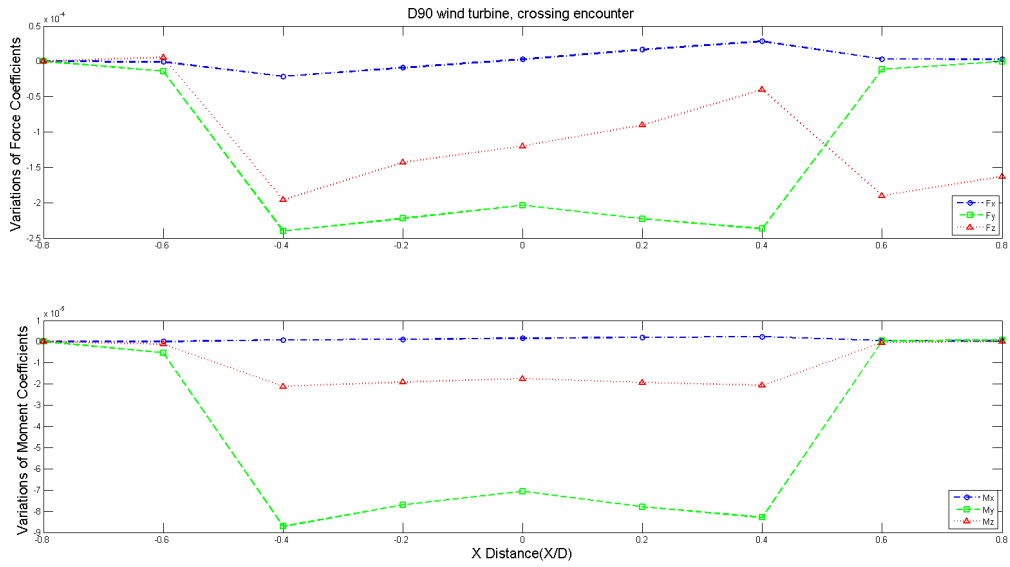
Figure 11: Variations of coefficients of forces and moments during off-line crossing wake encounter, GA flew along the runway Central line, offset 3D, model 1, normal core size, wind speed 32.8 ft/s.
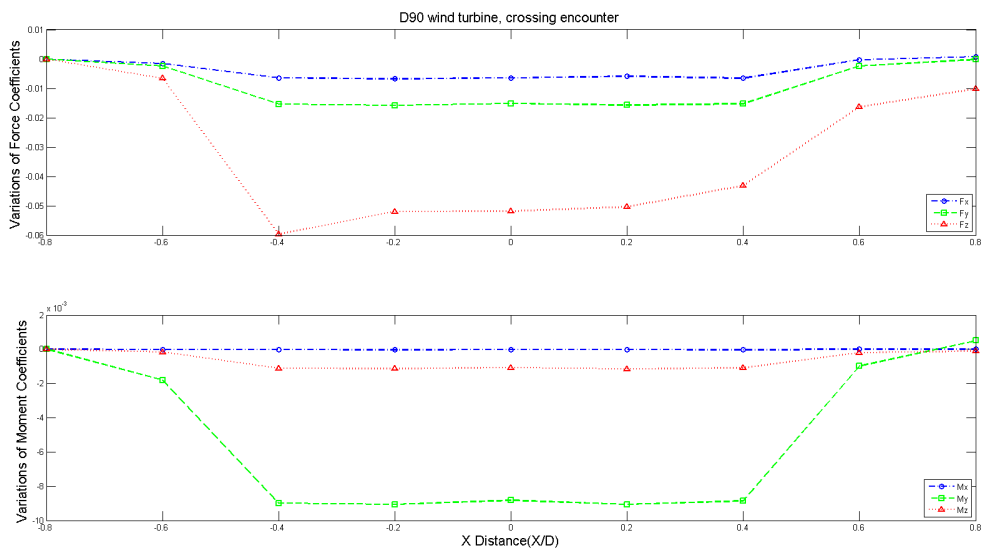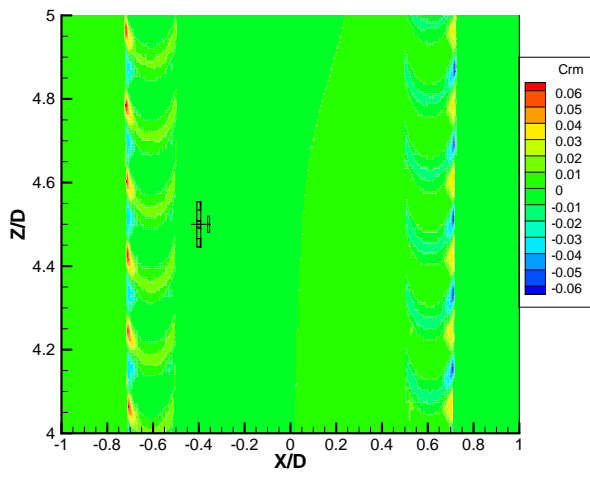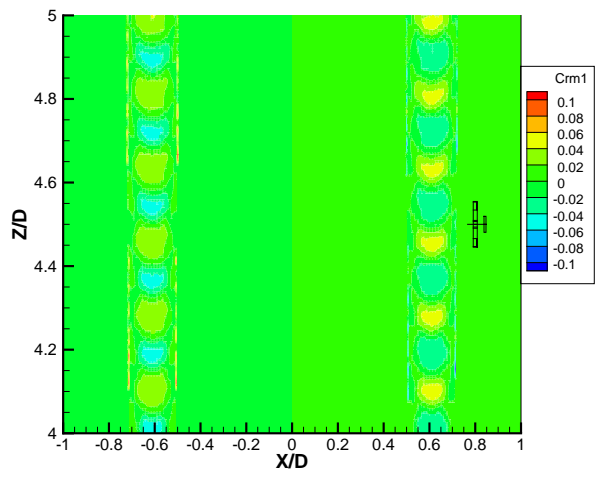

Figure 12: Variations of coefficients of forces and moments during off-line crossing wake encounter, GA flew along the runway central line, offset 3D, model 2, enlarged core size, wind speed 32.8 ft/s.

(a) Rolling moment coefficients induced by V_y (b) Rolling moment coefficients induced by V_x

Figure 13: Wake induced rolling moment coefficients of a large wind turbine with a 90 m diameter, model 2, wind speed 65.6 ft/s, the outline of the GA aircraft used for off-line flight simulations is also shown.